On the modeling of asymmetric yield functions

S.C. Soare[a,*], A.A. Benzerga[b]

[a]*Mechanical Eng. Department, Texas A&M Univ. at Qatar, Doha, Qatar*
[b]*Materials Science & Engineering Department, Texas A&M Univ., College Station, TX 77843, USA*

Abstract

A first degree homogeneous yield function is completely determined by its restriction to the unit sphere of the stress space; if, in addition, the function is isotropic and pressure independent, its restriction to an octahedric unit circle, the $\boldsymbol{\pi}$-circle, is periodic and determines uniquely the function. Thus any homogeneous, isotropic and pressure independent yield function can be represented by the Fourier series of its $\boldsymbol{\pi}$-circle restriction. Combinations of isotropic functions and linear transformations can then be used to extend the theory to anisotropic convex functions. The capabilities of this simple, yet quite general methodology are illustrated for the modeling of the yielding properties of AZ31B magnesium alloy.

Keywords: Yield surface, Asymmetry, Convexity, Fourier series, Trigonometric polynomials

1. Introduction

In the phenomenological theory of metal plasticity, plastic behavior is characterized by a yield surface/function and an associated flow rule. The initial yield surfaces of BCC and FCC alloys, e.g. steel and aluminum, are, within an acceptable approximation, symmetric with respect to the origin of the stress space. By contrast, the initial yield surfaces of HCP-metals are strongly asymmetric[1], due to asymmetries in yielding at constituent level, e.g., Bilby and Crocker (1965), Christian and Mahajan (1995), Balasubramanian and Anand (2002), Graff et al (2007), Kouchmeshky and Zabaras (2009). And even if initially symmetric, any yield surface may become asymmetric due to the residual stresses induced by plastic deformation, e.g. Ortiz and Popov (1983), Zatarin et al (2004), Barlat et al (2011).

While the description of symmetric yield surfaces is a relatively well developed subject, e.g. Barlat et al (2005), Banabic et al (2005), Barlat et al (2007), Soare and Barlat (2010), Huang and Man (2013), a general methodology for developing asymmetric yield functions is still lacking. As an early contribution, one may note the work of Liu et al (1997), where Hill's quadratic was extended via an algebraic combination of orthotropic extensions of the $J_2 := (1/2)|\boldsymbol{\sigma}'|$ and $I_1 := \mathrm{tr}(\boldsymbol{\sigma})$ invariants of the deviator of the stress tensor $\boldsymbol{\sigma}$. A similar approach was adopted later in Cazacu and Barlat (2004), where an algebraic combination of orthotropic extensions of J_2 and $J_3 := \det(\boldsymbol{\sigma}')$ was employed, and further extended to algebraic combinations of general homogeneous polynomials in Soare et al (2007). More recently, anisotropic extensions of particular isotropic pressure-dependent asymmetric functions were proposed by Plunkett et al (2008) and by Yoon et al (2014).

Most of the above anisotropic asymmetric functions are obtained by composing specific isotropic asymmetric functions with linear transformations of the stress tensor, Barlat et al (2007). As such, the modeling capabilities of the anisotropic function depend significantly on the isotropic generators employed. Here, we retain the linear transformation approach for generating anisotropic extensions, but aim at developing a general methodology for describing any isotropic and pressure-independent function, symmetric or not. This, in combination with a simple, geometrical method for constructing new isotropic functions, will allow us to exploit the linear transformation approach at its full potential. In a similar context, an early sketch of a general theory of ("plane-isotropic") yield functions, based on trigonometric polynomials, was outlined by Budianski (1984), although only for plane stress states and symmetric functions. We adopt the same approach, but develop the arguments down to the practical level where

*Corresponding author: stefancgsoare@yahoo.com

[1] In this work, *asymmetric* will always refer to the asymmetry with respect to the origin of the stress space.

applications can be developed with relative ease and in an algorithmic manner.

2. Isotropic, pressure-independent asymmetric yield functions for general stress states

We start with a brief review of the natural representation of isotropic functions, further details on this classic topic of plasticity can be found in Hill (1950). Let $\boldsymbol{\sigma}$ denote the stress tensor, $\boldsymbol{e}_i$ its principal directions, and σ_i its principal values. A pressure independent, first order positive homogeneous yield function f can be written as

$$f(\boldsymbol{\sigma}) = f(\boldsymbol{\sigma}') = |\boldsymbol{\sigma}'| f(\boldsymbol{\tau}') \tag{1}$$

where $|\boldsymbol{\sigma}| := \sqrt{\boldsymbol{\sigma}\cdot\boldsymbol{\sigma}}$ is the magnitude (or norm) of a second order tensor, $\boldsymbol{\sigma}' := \boldsymbol{\sigma} - \mathrm{tr}(\boldsymbol{\sigma})/3$ is the deviator of the stress $\boldsymbol{\sigma}$, and $\boldsymbol{\tau}' := \boldsymbol{\sigma}'/|\boldsymbol{\sigma}'|$ is its unit direction. Since the orientation of the principal frame $\{\boldsymbol{e}_i\}$ can be specified by, say, its three Euler angles ψ_i with respect to a material frame[2] , the analytic representation of f can be further detailed to

$$f(\boldsymbol{\sigma}) = |\boldsymbol{\sigma}'|\, g(\psi_1, \psi_2, \psi_3, \tau_1', \tau_2', \tau_3')$$

with τ_i' denoting the principal values of the direction of the stress deviator, related to those of $\boldsymbol{\sigma}$ by

$$\tau_i' = (\sigma_i - p)/|\boldsymbol{\sigma}'|, \quad \text{where} \quad p := \mathrm{tr}(\sigma)/3$$

In this section we shall be concerned with the representation of isotropic functions, functions that are invariant to any orthogonal transformation of the material axes. Then, by applying three successive rotations to the body, one can bring the material axes along the principal stress directions while leaving the yield function value unchanged; hence:

$$f(\boldsymbol{\sigma}) = |\boldsymbol{\sigma}'|\, g(\tau_1', \tau_2', \tau_3') \tag{2}$$

One can further apply a 90^o rotation of the body about the principal axis $\boldsymbol{e}_1$, leaving again the yield function value unchanged. This rotation switches the principal stresses σ_2 and σ_3. With two other 90^o rotations about $\boldsymbol{e}_2$ and $\boldsymbol{e}_3$ available, and the yield function invariant to any combination of them, it follows that the function g must be symmetric:

$$g(\tau_1', \tau_2', \tau_3') = g(\tau_2', \tau_1', \tau_3') = g(\tau_1', \tau_3', \tau_2') = \ldots \tag{3}$$

[2] A frame defined/oriented with respect to the material symmetries of the material.

Eqs (2) and (3) give the most general representation of an isotropic scalar function (with one symmetric tensor argument). However, the arguments of the g-function are not independent, since they are related by the two constraints $|\boldsymbol{\tau}'| = 1$ and $\tau_1' + \tau_2' + \tau_3' = 0$. With the $\boldsymbol{\pi}$-plane[3] defined by

$$\Pi_o := \{\boldsymbol{\sigma} \,|\, \sigma_1 + \sigma_2 + \sigma_3 = 0\}$$

of unit normal

$$\boldsymbol{n}_o = (\boldsymbol{e}_1 + \boldsymbol{e}_2 + \boldsymbol{e}_3)/\sqrt{3} \tag{4}$$

the yield function is completely determined by the restriction of the function g to the unit circle of the $\boldsymbol{\pi}$-plane, which will be referred to as the $\boldsymbol{\pi}$-circle. In geometric terms, the yield surface[4] $\overline{\sigma} = f(\boldsymbol{\sigma})$ is a cylinder with generatrices parallel to $\boldsymbol{n}_o$. Let θ denote the polar angle on the $\boldsymbol{\pi}$-circle, measured counterclockwise starting from, say, $\boldsymbol{g}_1$, where $\boldsymbol{g}_i$ denote the projections of $\boldsymbol{e}_i$ onto Π_o. Due to the symmetries in eq. (3), it is sufficient to consider only the restriction of g to the sector $[0, \pi/3]$ of the $\boldsymbol{\pi}$-circle, Fig. 1.

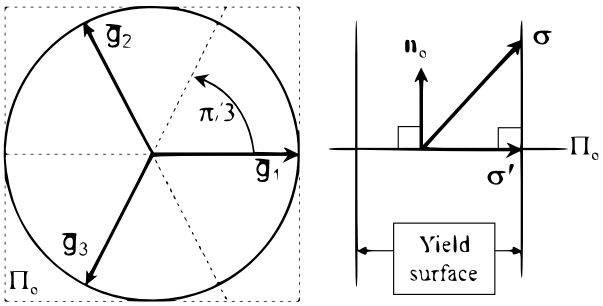

Figure 1: Projection of the principal stress frame onto the $\boldsymbol{\pi}$-plane (left), and orthogonal projection of the stress tensor onto the $\boldsymbol{\pi}$-plane of zero trace tensors (right).

Indeed, symmetry about $\boldsymbol{g}_1$ (actually, about the plane that contains $\boldsymbol{g}_1$ and is orthogonal to Π_o) reduces the range of θ from $[0, 2\pi]$ to $[0, \pi]$; the symmetry about $\boldsymbol{g}_2$ reduces it further to $[0, 2\pi/3]$; finally, the symmetry about $\boldsymbol{g}_3$ reduces the range of θ to $[0, \pi/3]$. Let $h = h(\theta)$ denote the restriction of g to the $\boldsymbol{\pi}$-circle. The final analytical expression for the yield function f, featuring the isotropy and pressure independence properties is then:

$$f(\boldsymbol{\sigma}) = |\boldsymbol{\sigma}'|\, h(\theta) \tag{5}$$

[3] Since only the principal stresses are of interest here, we may regard the stress tensor as a vector $\boldsymbol{\sigma} = \sigma_i \boldsymbol{e}_i$ of the 3D-space.

[4] For a given a hardening curve $\overline{\sigma} = \overline{\sigma}(\overline{\epsilon}^p)$, with $\overline{\epsilon}^p$ a measure of the magnitude of plastic deformation.

with $h : \mathbb{R} \longrightarrow \mathbb{R}_+$ uniquely determined by its restriction to the $[0, \pi/3]$ interval as follows: from $[0, \pi/3]$, h is extended into $[\pi/3, 2\pi/3]$ by symmetry (corresponding to the symmetry about $\boldsymbol{g}_3$); then h is extended to the interval $[0, 2\pi]$ by periodicity, with a $2\pi/3$-period; finally, h is extended from $[0, 2\pi]$ to the whole real axis by 2π-periodicity. Hence h is an even $2\pi/3$-periodic function. It can be represented, generally, as the cosine series:

$$h(\theta) = a_0/2 + \sum_{k\geq 1} a_k \cos(3k\theta) \tag{6}$$

The $\boldsymbol{\pi}$-plane projections $\boldsymbol{g}_i = \boldsymbol{e}_i - \boldsymbol{n}_o/\sqrt{3}$ have unit directions $\overline{\boldsymbol{g}}_i := \sqrt{3/2}\,\boldsymbol{g}_i$ and the deviator admits the representation $\boldsymbol{\sigma}' = \sigma_i \boldsymbol{e}_i - p\sqrt{3}\,\boldsymbol{n}_o = \sqrt{2/3}\,\sigma_i\,\overline{\boldsymbol{g}}_i$. The angle θ associated with a stress state $\boldsymbol{\sigma} = \sigma_i \boldsymbol{e}_i$ is then calculated from $\cos\theta = \overline{\boldsymbol{g}}_1 \cdot \boldsymbol{\sigma}'/|\boldsymbol{\sigma}'|$, that is

$$\theta = \operatorname{acos} \frac{2\sigma_1 - \sigma_2 - \sigma_3}{|\boldsymbol{\sigma}'|\sqrt{6}} \tag{7}$$

Conversely, given an angle θ and the magnitude of the deviator, from the representations $\sigma'_i \boldsymbol{e}_i = \boldsymbol{\sigma}' = |\boldsymbol{\sigma}'|(\cos\theta\,\overline{\boldsymbol{g}}_1 + \sin\theta\,\boldsymbol{q})$, where $\boldsymbol{q} := (\overline{\boldsymbol{g}}_2 - \overline{\boldsymbol{g}}_3)/|\overline{\boldsymbol{g}}_2 - \overline{\boldsymbol{g}}_3|$ is such that $\overline{\boldsymbol{g}}_1$ and $\boldsymbol{q}$ form an orthogonal basis in the $\boldsymbol{\pi}$-plane, associated with the polar coordinates[5] $|\boldsymbol{\sigma}'|$ and θ, one deduces the components of the deviator $\boldsymbol{\sigma}'$:

$$\begin{aligned}
\sigma'_1 &= |\sigma'|\sqrt{\frac{2}{3}}\cos(\theta) \\
\sigma'_2 &= \frac{|\sigma'|}{\sqrt{2}}\left(\sin\theta - \frac{\cos\theta}{\sqrt{3}}\right) = |\sigma'|\sqrt{\frac{2}{3}}\cos(\theta + 4\pi/3) \\
\sigma'_3 &= \frac{-|\sigma'|}{\sqrt{2}}\left(\sin\theta + \frac{\cos\theta}{\sqrt{3}}\right) = |\sigma'|\sqrt{\frac{2}{3}}\cos(\theta + 2\pi/3)
\end{aligned} \tag{8}$$

We note that $\sigma'_1 \geq \sigma'_2 \geq \sigma'_3$ if and only if $0 \leq \theta \leq \pi/3$.

To complete the theory of eqs.(5)-(8), conditions must be given for the parameters a_k so that the yield function be convex. It is shown in Appendix A that these are

$$\begin{aligned}
&h''(\theta) + h(\theta) \geq 0, \forall\theta \in [0, \pi/3] \iff \\
&a_0/2 + \textstyle\sum_{k\geq 1} a_k \left(1 - 9k^2\right)\cos(3k\theta) \geq 0, \forall\theta \in [0, \pi/3]
\end{aligned} \tag{9}$$

For a fixed $\theta \in [0, \pi/3]$, the second inequality above defines a half-space in the a_k-space. With θ covering the $[0, \pi/3]$ interval, the convexity domain for a_k is an intersection of half-planes, and hence the convexity domain itself is a convex subset in the a_k-space.

2.1. Illustrations

That Fourier series can represent a wide class of functions is well known. The question is whether this representation is efficient for yield functions. Most of the yield criteria have analytical representations in the form of smooth functions[6], at least of class C^1. Hence the Fourier series expansions of their corresponding h-functions should converge relatively fast. Equivalently, sufficiently smooth yield functions should accept accurate approximations within a subspace of trigonometric polynomials of reasonably small dimension. It is then instructive to illustrate here the trigonometric representation of other analytical formulations.

With eqs.(5) and (8), the h-function of a homogeneous isotropic pressure-independent yield function f is

$$h(\theta) = \sqrt{\frac{2}{3}}\, f(\cos\theta, \cos(\theta + 4\pi/3), \cos(\theta + 2\pi/3)) \tag{10}$$

and the coefficients of its Fourier expansion are calculated by

$$a_k = \frac{6}{\pi}\int_0^{\pi/3} h(\theta)\cos(3k\theta), k \geq 0 \tag{11}$$

The Hershey (1954)-Hosford (1972) isotropic yield function reads

$$f^a(\boldsymbol{\sigma}) = K\left[(\sigma_1 - \sigma_2)^a + (\sigma_2 - \sigma_3)^a + (\sigma_3 - \sigma_1)^a\right] \tag{12}$$

with a an even natural number and $K = 1/2$ the normalization constant along uniaxial traction. It is symmetric and hence its h-function is even $\pi/3$-periodic; with eqs.(10) and (11), the first few terms of its Fourier expansion, in the case $a = 8$, are

$$\begin{aligned}
h(\theta) = \frac{2.52657}{2} &- \frac{3.65434}{10^2}\cos(6\theta) - \frac{1.8511}{10^3}\cos(12\theta) \\
&- \frac{1.3397}{10^4}\cos(18\theta) - \frac{1.115}{10^5}\cos(24\theta) - ...
\end{aligned}$$

A second example is the asymmetric isotropic function studied by Cazacu et al (2006):

$$f^a(\boldsymbol{\sigma}) = K\left[(|\sigma'_1| - c\sigma'_1)^a + (|\sigma'_2| - c\sigma'_2)^a + \left(|\sigma'_3| - c\sigma'_3\right)^a\right]$$

where $c \in [-1, 1]$, the convexity interval, $a \geq 1$, and $K := 1/\left[2^a(1-c)^a + 2(1+c)^a\right]$ is the normalization constant along uniaxial traction. When $c = 0$ this function is symmetric and generates only biaxial curves that either coincide with Mises ($a = 2$), or are exterior to the von Mises oval. For $c = 0.8$ and $a = 4$, with eqs.(10)

[5] Often referred to as the Haigh-Westergaard parametrization

[6] Tresca's yield function being a notable exception

and (11), the first coefficients of the series representation eq.(6) of its *h*-function are reported in the CPB-column of Table C.1 of Appendix C.

The biaxial curves of both functions, approximated by retaining the first 5 and 18 terms, respectively, of their Fourier series are drawn in Fig. 2. As truncation criterion, enough terms were retained so that the maximum of the absolute value of the difference between original and approximate be of the order of $1/10^5$ while retaining convexity.

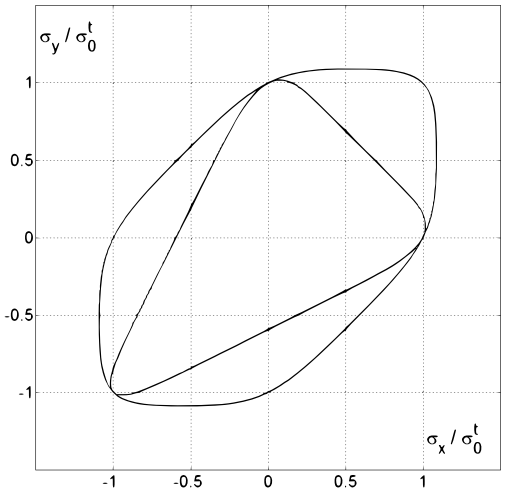

Figure 2: Biaxial curves of the symmetric Hershey-Hosford and asymmetric CPB06 yield functions, respectively, in trigonometric representation.

2.2. Designing two-parameters yield functions

As the previous illustrations have shown, trigonometric polynomials can provide accurate representations of isotropic yield functions. However, not every such polynomial is suitable for yield function representation. Here we show a method for parameterizing a relevant subset of a space of trigonometric polynomials. In addition, while the $\boldsymbol{\pi}$-plane is well suited for theoretical developments, the restriction of the yield function to biaxial stress states provides a more intuitive picture. Therefore, rather than using an arc of the $\boldsymbol{\pi}$-circle, we shall use instead a segment of the biaxial curve[7] to construct isotropic functions.

Several yielding points are of interest; with eq.(7):
1)*Uniaxial traction*: $\sigma = (\sigma_0^t, 0, 0)$, with $\sigma_0^t > 0$; then $\sigma'_1 = 2\sigma_0^t/3 > -\sigma_0^t/3 = \sigma'_2 = \sigma'_3$ and hence $\cos\theta = 1$ so that $\theta = 0$.
2)*Uniaxial compression*: $\sigma = -(\sigma_0^c, 0, 0)$, with $\sigma_0^c > 0$; then $\sigma'_1 = \sigma'_2 = \sigma_0^c/3 > -2\sigma_0^c/3 = \sigma'_3$ and hence $\cos\theta = 1/2$ so that $\theta = \pi/3$.
3)*Balanced-biaxial traction*: $\sigma = (\sigma_b^t, \sigma_b^t, 0)$, with $\sigma_b^t > 0$; then $\sigma'_1 = \sigma'_2 = \sigma_b^t/3 > -2\sigma_b^t/3 = \sigma'_3$ and hence $\cos\theta = 1/2$ so that $\theta = \pi/3$. It necessarily follows that for any isotropic function there holds: $\sigma_0^c = \sigma_b^t$.
4)*Balanced-biaxial compression*: $\sigma = -(\sigma_b^c, \sigma_b^c, 0)$, with $\sigma_b^c > 0$; then $\sigma'_1 = 2\sigma_b^c/3 > -\sigma_b^c/3 = \sigma'_2 = \sigma'_3$ and hence $\cos\theta = 1$ so that $\theta = 0$. Thus for any isotropic function there holds: $\sigma_0^t = \sigma_b^c$.
5)*Biaxial traction*: $\sigma = (\sigma_a, \sigma_a/2, 0)$, with $\sigma_a > 0$; then $\sigma'_1 = \sigma_a/2 > 0 = \sigma'_2 > -\sigma_a/2 = \sigma'_3$ and hence $\cos\theta = \sqrt{3}/2$ so that $\theta = \pi/6$.
6)*Pure shear*: $\sigma = (\sigma_s, -\sigma_s, 0)$, with $\sigma_s > 0$; then $\cos\theta = \sqrt{3}/2$ so that $\theta = \pi/6$. Thus for any isotropic function there holds: $\sigma_s = \sigma_a/2$.

More generally, if the biaxial stress state is described by $\sigma_1 = \rho\cos\psi$, $\sigma_2 = \rho\sin\psi$, then the biaxial angle ψ and the angle θ on the $\boldsymbol{\pi}$-circle are related by

$$\tan\psi = \frac{\sin^2\theta \pm \sin 2\theta\,\sqrt{3}/2}{4\sin^2\theta - 3} \tag{13}$$

The "plus" branch of the above formula is a one-to-one map of $\theta \in [0, \pi/3)$ onto $\psi \in [0, \pi/4)$, and hence, by symmetry reasons alone, the compression part of the biaxial curve is completely determined by the tensile part. The "minus" branch of the formula is a one-to-one map of $\theta \in [0, \pi/3)$ onto $\psi \in (-\pi/2, 0]$, and hence the shear part of the biaxial curve could also be used as a generating sector.

In particular, from the above list, three[8] modeling points have characterizing properties, say 1), 3), and 5). Then a three-parameter *h*-function can be represented in the form:

$$h(\theta) = p_0 + p_1\phi_1(\theta) + p_2\phi_2(\theta) \tag{14}$$

where ϕ_1 and ϕ_2 are suitably chosen shape (or basis) functions.

In eq.(14), p_0, p_1 and p_2 are parameters which are reduced, upon normalization, to two independent shape-parameters as follows. The three equations characterizing yielding in the loading modes 1), 3) and 5), are, respectively,

$$\begin{aligned} &p_0 + \phi_{11}p_1 + \phi_{21}p_2 = t_1\sqrt{3/2}, \quad \text{with } t_1 := \overline{\sigma}/\sigma_0^t \\ &p_0 + \phi_{12}p_1 + \phi_{22}p_2 = t_2\sqrt{3/2}, \quad \text{with } t_2 := \overline{\sigma}/\sigma_b^t \\ &p_0 + \phi_{13}p_1 + \phi_{23}p_2 = t_3\sqrt{2}, \quad \text{with } t_3 := \overline{\sigma}/\sigma_a \end{aligned} \tag{15}$$

[7] A section through the yield surface by, say, the (σ_1, σ_2)-plane.

[8] Other modeling points can be added as needed, as for example the tensile stress of direction $(1, 1/4, 0)$.

where it has been denoted $\phi_{11} := \phi_1(0)$, $\phi_{21} := \phi_2(0)$, $\phi_{12} := \phi_1(\pi/3)$, $\phi_{22} := \phi_2(\pi/3)$, $\phi_{13} := \phi_1(\pi/6)$, $\phi_{23} := \phi_2(\pi/6)$. Denoting

$$\Delta := (\phi_{12} - \phi_{11})(\phi_{23} - \phi_{21}) + (\phi_{11} - \phi_{13})(\phi_{22} - \phi_{21})$$

and $\bar{t}_1 := t_1\sqrt{3/2}$, $\bar{t}_2 := t_2\sqrt{3/2}$, $\bar{t}_3 := t_2\sqrt{2}$, it follows:

$$\begin{aligned} p_0 &= \bar{t}_1 - \phi_{11}p_1 - \phi_{21}p_2 \\ p_1 &= \frac{1}{\Delta}\left[(\phi_{23} - \phi_{21})(\bar{t}_2 - \bar{t}_1) + (\phi_{22} - \phi_{21})(\bar{t}_1 - \bar{t}_3)\right] \\ p_2 &= \frac{1}{\Delta}\left[(\phi_{13} - \phi_{11})(\bar{t}_1 - \bar{t}_2) + (\phi_{12} - \phi_{11})(\bar{t}_3 - \bar{t}_1)\right] \end{aligned} \quad (16)$$

In what follows, the usual scaling of the yield function with σ_0^t will be used and then $t_1 = 1$. Hence, the two parameters of the h-function in eq.(14) are the ratios t_2 and t_3. They can vary only within an admissible domain where the resulting yield function is convex, the convexity domain. This domain is characterized by eq.(9), which in the present case reduces to, by substituting eq.(16) into eq.(14):

$$\alpha(\theta)t_2 + \beta(\theta)t_3 \geq \gamma(\theta), \forall\theta \in [0, \pi/3] \quad (17)$$

where

$$\begin{aligned} \alpha &:= (\phi_{11} - d_1)(\phi_{21} - \phi_{23}) + (\phi_{21} - d_2)(\phi_{13} - \phi_{11}) \\ \beta &:= (\phi_{11} - d_1)(\phi_{22} - \phi_{21}) + (\phi_{21} - d_2)(\phi_{11} - \phi_{12}) \\ \gamma &:= \Delta + (\phi_{11} - d_1)(\phi_{23} - \phi_{22}) + (\phi_{21} - d_2)(\phi_{12} - \phi_{13}) \end{aligned}$$

and $d_i(\theta) := \phi_i(\theta) + \phi_i''(\theta)$, $i = 1, 2$.

The inequalities in (17) define the convexity domain in the (t_2, t_3)-plane, each inequality, corresponding to some $\theta \in [0, \pi/3]$, describing a half-plane containing the convexity domain. It is never empty, since the Mises quadratic corresponds to the pair $(t_2 = 1, t_3 = \sqrt{3}/2 \approx 0.866)$. However, the size and spread of the convexity domain about the point $(1, 0.866)$, and hence the modeling range of formula (14), depend considerably on the choice of the basis functions ϕ_i.

2.2.1. Constructing basis functions

The ϕ_i-functions in eq.(14) are constructed as h-functions of yield functions that have as traces on the biaxial plane conveniently chosen biaxial curves. To this end we assume that the relevant arc of the latter (by eq.(13), spanning the $[0, \pi/4]$ sector of the first quadrant) is represented in the implicit form

$$\phi(\sigma_x, \sigma_y) = 1 \quad (18)$$

with ϕ a symmetric and first degree positive homogeneous function; with the polar parametrization $\sigma_x = \rho\cos\psi$ and $\sigma_y = \rho\sin\psi$ of the biaxial plane (σ_x, σ_y), the above is equivalent to

$$\rho(\psi) = 1/\phi(\cos\psi, \sin\psi) \quad (19)$$

Assuming that this biaxial curve is the trace of a yield function f on the (σ_x, σ_y)-plane, recalling eq.(5) there holds

$$h(\theta) = \frac{f(\sigma_x, \sigma_y, 0, ...)}{|(\sigma_x, \sigma_y, 0, ...)'|} = \frac{\phi(\sigma_x, \sigma_y)}{|(\sigma_x, \sigma_y, 0, ...)'|}$$

and defining $\bar{h}(\psi) := \phi(\cos\psi, \sin\psi)$, the restriction of ϕ to the unit circle of the (σ_x, σ_y)-plane, it follows

$$h(\theta) = \frac{\bar{h}(\psi)\sqrt{3/2}}{\sqrt{1 - \cos\psi\sin\psi}} = \frac{\sqrt{3/2}}{\rho(\psi)\sqrt{1 - \cos\psi\sin\psi}} \quad (20)$$

With eq.(13) providing a one-to-one map $[0, \pi/3] \ni \theta \longrightarrow \psi \in [0, \pi/4]$, the above formula calculates the h-function in terms of the $[0, \pi/4]$-arc a biaxial curve. Of course, not just any biaxial curve is the trace of an isotropic yield function. For C^1-smooth functions the biaxial curve must satisfy the following condition [9]

$$\frac{\partial\phi}{\partial\sigma_x}(1, 0) + 2\frac{\partial\phi}{\partial\sigma_y}(1, 0) = 0 \quad (21)$$

The biaxial function is taken in the form of a patch of two C^2-smooth, symmetric and positive homogeneous functions. As shown next, this will allow for sufficient modeling flexibility with the advantage of retaining simplicity in calculations. Then defining the stress ratio $t := \sigma_y/\sigma_x$,

$$\phi(\sigma_x, \sigma_y) = \begin{cases} \phi^{(1)}(\sigma_x, \sigma_y), & \text{if } 0 \leq t \leq t^* \\ \phi^{(2)}(\sigma_x, \sigma_y), & \text{if } t^* \leq t \leq 1 \end{cases} \quad (22)$$

where t^* is a stress ratio serving as parameter of the patch. Furthermore, the patch is subjected to the condition that it be C^2-smooth at the contact point $\sigma_x^*(1, t^*)$. This translates into three relations as follows. First, continuity demands that:

$$\phi^{(2)}(1, t^*) = \phi^{(1)}(1, t^*) \quad (23)$$

Second, the curve defined by the patch may also be parameterized, arbitrarily for the moment, in the form $\sigma_x = \sigma_x(s)$ and $\sigma_y = \sigma_y(s)$ with the parameter s in a certain interval; substituting in eq.(18) and differentiating with respect to s obtains

$$\frac{\partial\phi}{\partial\sigma_x}(\sigma_x(s), \sigma_y(s))\frac{d\sigma_x}{ds} + \frac{\partial\phi}{\partial\sigma_y}(\sigma_x(s), \sigma_y(s))\frac{d\sigma_y}{ds} = 0 \quad (24)$$

[9] Stating that the r-value of ϕ is one. This is further equivalent with the symmetry condition $h'(0) = 0$; the proof is straightforward but rather technical and therefore is not included here.

relationship holding at all points s for which $t(s) := \sigma_y(s)/\sigma_x(s) \neq t^*$. Then the limits $t(s) \uparrow t^*$ and $t(s) \downarrow t^*$ provide two relationships that, when subtracted, result in the following condition for a C^1-smooth contact:

$$\frac{\partial\phi^{(2)}}{\partial\sigma_x}(1,t^*)\Lambda+\frac{\partial\phi^{(2)}}{\partial\sigma_y}(1,t^*) = \frac{\partial\phi^{(1)}}{\partial\sigma_x}(1,t^*)\Lambda+\frac{\partial\phi^{(1)}}{\partial\sigma_y}(1,t^*) \quad (25)$$

Above, we used the first degree homogeneity of the $\phi^{(i)}$ functions and defined $\Lambda := (d\sigma_x/d\sigma_y)(s^*)$, s^* denoting the value of s corresponding to t^*.

Differentiating with respect to s the relationship in eq.(24) obtains, for all $s \neq s^*$

$$\frac{\partial^2\phi}{\partial\sigma_x^2}\left(\frac{d\sigma_x}{ds}\right)^2 + 2\frac{\partial^2\phi}{\partial\sigma_x\partial\sigma_y}\frac{d\sigma_x}{ds}\frac{d\sigma_y}{ds} + \frac{\partial^2\phi}{\partial\sigma_y^2}\left(\frac{d\sigma_y}{ds}\right)^2 + \frac{\partial\phi}{\partial\sigma_x}\frac{d^2\sigma_x}{ds^2} + \frac{\partial\phi}{\partial\sigma_y}\frac{d^2\sigma_y}{ds^2} = 0$$

For $s = s^*$, we can now choose a parametrization such that[10]

$$\left(\frac{\partial\phi^{(2)}}{\partial\sigma_x} - \frac{\partial\phi^{(1)}}{\partial\sigma_x}\right)\frac{d^2\sigma_x}{ds^2} + \left(\frac{\partial\phi^{(2)}}{\partial\sigma_y} - \frac{\partial\phi^{(1)}}{\partial\sigma_y}\right)\frac{d^2\sigma_y}{ds^2} = 0$$

without altering the Λ-ratio. With the last two relationships, and using once again the homogeneity of the ϕ functions, a C^2-smooth contact implies

$$\left[\frac{\partial^2\phi^{(2)}}{\sigma_x^2}\Lambda^2 + 2\frac{\partial^2\phi^{(2)}}{\partial\sigma_x\partial\sigma_y}\Lambda + \frac{\partial^2\phi^{(2)}}{\partial\sigma_y^2}\right](1,t^*) = \left[\frac{\partial^2\phi^{(1)}}{\sigma_x^2}\Lambda^2 + 2\frac{\partial^2\phi^{(1)}}{\partial\sigma_x\partial\sigma_y}\Lambda + \frac{\partial^2\phi^{(1)}}{\partial\sigma_y^2}\right](1,t^*) \quad (26)$$

Here, the functions $\phi^{(i)}$ are taken in the form of symmetric homogeneous polynomials of degree six

$$\phi^{(i)} = a_1^{(i)}\left(\sigma_x^6+\sigma_y^6\right) + a_2^{(i)}\left(\sigma_x^5\sigma_y+\sigma_x\sigma_y^5\right) + a_3^{(i)}\left(\sigma_x^4\sigma_y^2+\sigma_x^2\sigma_y^4\right) + a_4^{(i)}\sigma_x^3\sigma_y^3 \quad (27)$$

The biaxial curve is then constructed as follows. First, $\phi^{(1)}$ is determined by the r-value condition in eq.(21), the equations

$$\phi(1,0) = 1,\ \phi(1,t^*) = 1/(\sigma_x^*)^6$$

stating that the biaxial curve passes through the points $(1,0)$ and $(\sigma_x^*, t^*\sigma_x^*)$, and

$$\frac{\partial\phi^{(1)}}{\partial\sigma_x}(1,t^*)\Lambda + \frac{\partial\phi^{(1)}}{\partial\sigma_y} = 0$$

stating that the biaxial curve has a slope $1/\Lambda$ at point $(\sigma_x^*, t^*\sigma_x^*)$. Then, the second branch of the patch is determined by the C^2-smoothness conditions in eqs.(23,25,26), and the additional equation:

$$\phi^{(2)}(1,1) = 1/\sigma_b^6 \quad (28)$$

stating that the biaxial curve passes through the balanced-biaxial stress point (σ_b, σ_b).

All these equations are linear and determine the $a_k^{(i)}$-coefficients once the parameters of the Poly6-patch, t^*, σ_x^*, Λ and σ_b are given[11]. The parameter σ_b characterizes the type and the degree of tension-compression asymmetry of the biaxial curve, while Λ, t^* and σ_x^* further modulate its shape.

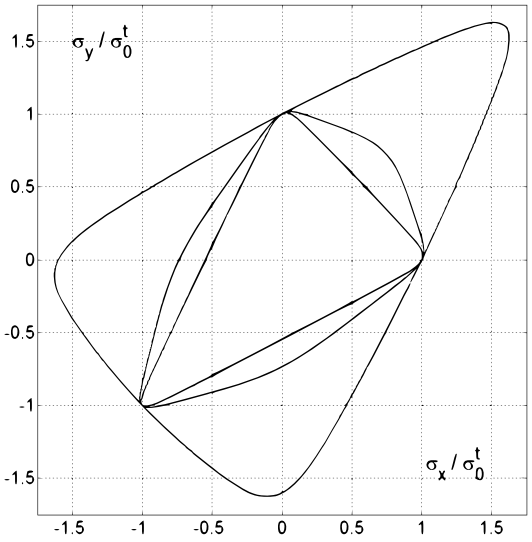

Figure 3: Biaxial curves generated using the Poly6-patch; illustrations for $\sigma_b \in \{0.5472, 0.736, 1.6\}$

The domain of variation of these parameters is restricted by the requirement that the biaxial curve be convex. Admissible values can be found by a trial and error procedure as follows. Given a triplet $(t^*, \sigma_x^*, \Lambda)$, one varies σ_b within an appropriate interval (for example, if biaxial curves with a compression/tension ratio less than one are sought, the maximal interval of variation for σ_b is $(0.5, 1)$); for each σ_b, one calculates the coefficients of the patch, then the Fourier coefficients of the

[10] In geometric terms: assuming the contact is already C^1-smooth, the velocity vector is orthogonal on both gradients $\nabla\phi^{(1)}$ and $\nabla\phi^{(2)}$; by parameterizing the curve so that the acceleration and velocity are collinear at $s = s^*$, there holds $\left(\nabla\phi^{(2)} - \nabla\phi^{(1)}\right)\cdot(d^2/ds^2)\left(\sigma_x, \sigma_y\right) = 0$.

[11] One could also consider a patch of two homogeneous polynomials of degree four; in this case, the C^2-smooth contact condition would make $\phi^{(1)}$ and $\phi^{(2)}$ identical, since each have three parameters. Instead, a C^1-smooth Poly4-patch has two parameters, e.g., σ_b and σ_x^*, assuming t^* fixed (Λ can be calculated once $\phi^{(1)}$ is known)

h-function via eq.(20), and finally checks the convexity of the yield function via the relationships in eq.(9). In this way, one determines the subinterval of admissible values of σ_b for which the generated yield function is convex; in case this convexity subinterval is empty, the current triplet $(t^*, \sigma_x^*, \Lambda)$ is not admissible and a new estimate of $(t^*, \sigma_x^*, \Lambda)$ may be tested, etc.

Examples of biaxial curves generated with the Poly6-patch are shown in Fig. 3. Some parameters values and σ_b-intervals of convexity are as follows:
$t^* = 0.145$, $\Lambda = -0.9$, $\sigma_x^* = 0.945$, $0.5471 \leq \sigma_b \leq 0.5526$;
$t^* = 0.15$, $\Lambda = -0.3$, $\sigma_x^* = 1.0$, $0.6441 \leq \sigma_b \leq 0.7361$;
$t^* = 0.5$, $\Lambda = -0.45$, $\sigma_x^* = 1.31$, $1.2535 \leq \sigma_b \leq 1.65$.

Since we envision applications to the modeling of magnesium alloys, and since these have, in general, a compression to tension ratio of less than one, a two-parameter isotropic function, $f(\boldsymbol{\sigma}) = |\boldsymbol{\sigma}'|h(\theta)$ with the h-function given by eq.(14), is constructed by defining ϕ_1 to be the h-function of the Hershey-Hosford yield function with an exponent $a = 30$ in eq.(12), and ϕ_2 to be the h-function of the Poly6-patch curve with parameters $t^* = 0.145$, $\Lambda = -0.9$, $\sigma_x^* = 0.945$, $\sigma_b = 0.5472$, the small "triangle" in Fig. 3. The coefficients of the trigonometric representations of ϕ_1 and ϕ_2 are featured in the columns "HH" and "Poly6" of Table C.1 of Appendix C.

Given the ϕ_1 and ϕ_2 functions, using the convexity constraints in eq.(17), the convexity domain for the t_2 and t_3 parameters of the function can be obtained in graphic form by plotting the (linear) constraints corresponding to a fine set of sampling points $\theta_k \in [0, \pi/3]$. The white region in Fig. 4 represents the convexity domain of the particular isotropic function constructed above.

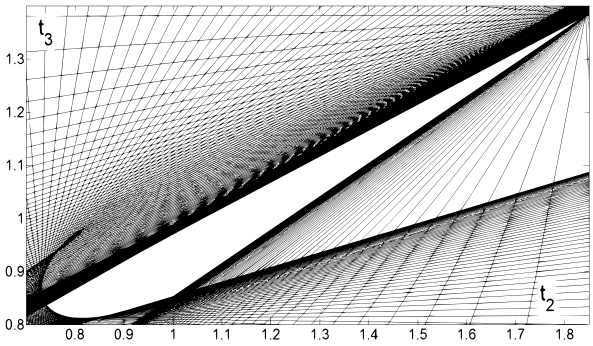

Figure 4: Convexity domain in the (t_2, t_3)-plane.

It can be noticed that it contains functions with opposite asymmetry (compression/tension ratio greater than one, for $t_2 < 1$) even though both ϕ_1 and ϕ_2 have $t_2 \geq 1$. The shape of the convexity domain is simple enough to be generated by just a few vertices. Simple inspection identifies the following points of interest: $(1.8303, 1.3741)$, $(1.0, 0.9696)$, $(0.742, 0.836)$, $(0.81, 0.813)$, $(1.0, 0.85285)$. The convex hull of the set formed by these points can then serve as an approximation from within of the convexity domain.

3. Anisotropic extensions

As announced in the introductory section, we shall use next the linear transformation approach to obtain anisotropic yield functions. Since this approach employs quite a particular parametrization of the symmetry group, one cannot expect that every anisotropic function can be satisfactorily approximated. On the other hand, convexity is assured by default, which is an important advantage for the parameters-identification procedure[12].

Given N_I isotropic, pressure-independent and positive homogeneous of first degree (convex) yield functions $g^{(i)}$, an anisotropic, pressure-independent and positive homogeneous convex function $\hat{f}$ is obtained by defining

$$\hat{f}(\boldsymbol{\sigma}) := \sum_{i=1}^{N_I} g^{(i)}(\boldsymbol{\Sigma}^{(i)}) \tag{29}$$

where

$$\boldsymbol{\Sigma}^{(i)} := \boldsymbol{A}^{(i)} : \boldsymbol{\sigma}' \tag{30}$$

and $\boldsymbol{A}^{(i)}$ are fourth order tensors which are invariant to the symmetry group of the material. If $\boldsymbol{\sigma_0} := \overline{\sigma}\boldsymbol{\tau}$ represents a uniaxial state of tensile stress along the unit stress-direction $\boldsymbol{\tau}$, by defining

$$K := \hat{f}(\boldsymbol{\tau}) \tag{31}$$

a normalized anisotropic yield function is defined by

$$f(\boldsymbol{\sigma}) := \frac{1}{K}\hat{f}(\boldsymbol{\sigma}) \tag{32}$$

having the property that $f(\boldsymbol{\sigma_0}) = \overline{\sigma} = |\boldsymbol{\sigma_0}|$, the magnitude of the uniaxial stress.

For orthotropic symmetry, the case of most interest in applications, a generic linear transformation as in

[12] Which becomes a constrained optimization problem in the absence of default convexity.

eq.(30) acquires, with respect to the material frame[13], the component form[14]

$$\begin{aligned}
\Sigma_{11} &= a_1\sigma_{11} + a_2\sigma_{22} - (a_1+a_2)\sigma_{33}\\
\Sigma_{22} &= a_3\sigma_{11} + a_4\sigma_{22} - (a_3+a_4)\sigma_{33}\\
\Sigma_{33} &= -\Sigma_{11} - \Sigma_{22}\\
\Sigma_{12} &= a_5\sigma_{12},\ \ \Sigma_{13} = a_6\sigma_{13},\ \ \Sigma_{23} = a_7\sigma_{23}
\end{aligned} \tag{33}$$

The principal values of a generic *deviatoric* image stress $\boldsymbol{\Sigma}$ are calculated by, e.g., Malvern (1969),

$$\Sigma_i = 2\sqrt{J_2(\boldsymbol{\Sigma})/3}\cos\gamma_i \tag{34}$$

where

$$\gamma_1 := \frac{1}{3}\text{acos}\left[\frac{J_3(\boldsymbol{\Sigma})}{2}\left(\frac{3}{J_2(\boldsymbol{\Sigma})}\right)^{3/2}\right],$$
$$\gamma_2 := \gamma_1 + 2\pi/3,\ \ \gamma_3 := \gamma_2 + 2\pi/3$$

and

$$J_2(\boldsymbol{\Sigma}) := \frac{1}{2}|\boldsymbol{\Sigma}|^2,\ \ J_3(\boldsymbol{\Sigma}) := \det(\boldsymbol{\Sigma}) \tag{35}$$

Finally, the angle on the $\boldsymbol{\pi}$-circle is calculated by the formula in eq.(7) and the value of the yield function on the given stress state $\boldsymbol{\sigma}$ is calculated using eq.(32) and the natural representation of the isotropic generators in eqs.(5) and (6). Formulas for the gradient of the yield function are provided in Appendix B.

3.1. Application to the modeling of Mg-alloy orthotropic sheet

In what follows, the modeling range of eqs.(29)-(33) is tested on the AZ31B Mg-sheet, a material featuring a very high tension-compression asymmetry. With the material frame axes 1, 2 and 3 (or x, y and z) aligned along the rolling, transverse and thickness directions, respectively, the usual experimental characterization of orthotropic sheet provides a set of directional yield stresses, that is, magnitudes σ_θ of uniaxial stress states $\boldsymbol{\sigma_\theta} := \sigma_\theta\boldsymbol{\tau_\theta}$, along loading directions[15] $\boldsymbol{v_\theta} := \pm(\cos\theta, \sin\theta, 0)$ in the sheet plane,

$$\sigma_\theta = \frac{\overline{\sigma}}{f(\boldsymbol{\tau_\theta})} \tag{36}$$

and corresponding directional r-values (the gradient of the yield function is calculated in Appendix B)

$$r_\theta := \frac{D^p_{\theta+\pi/2}}{D^p_{33}} = \frac{\left(\dfrac{\partial\hat{f}}{\partial\boldsymbol{\sigma}}(\boldsymbol{\tau_\theta}) : \boldsymbol{v}^{\perp}_{\boldsymbol{\theta}}\right)\cdot\boldsymbol{v}^{\perp}_{\boldsymbol{\theta}}}{\dfrac{\partial\hat{f}}{\partial\sigma_{11}}(\boldsymbol{\tau_\theta}) + \dfrac{\partial\hat{f}}{\partial\sigma_{22}}(\boldsymbol{\tau_\theta})} \tag{37}$$

where, assuming the normality rule, $\boldsymbol{D}^p = \dot{\lambda}\,\partial f/\partial\boldsymbol{\sigma}$ is the rate of plastic deformation, $\boldsymbol{v}^{\perp}_{\boldsymbol{\theta}} := (-\sin\theta, \cos\theta, 0)$, and

$$\boldsymbol{\tau_\theta} := \pm\begin{bmatrix}\cos^2\theta & \sin\theta\cos\theta & 0\\ \sin\theta\cos\theta & \sin^2\theta & 0\\ 0 & 0 & 0\end{bmatrix}$$

the + and − signs corresponding to tension and compression, respectively.

Throughout the rest of this section the yield function is normalized with the yield stress along the rolling direction and hence the normalization constant in eq.(31) is $K = \hat{f}(\boldsymbol{\tau_0})$, with $\boldsymbol{\tau_0} = \text{diag}[1, 0, 0]$.

A more detailed description of the plastic properties of the sheet is obtained by testing sheet samples under tensile in-plane biaxial stressing conditions to obtain, for example, values $\sigma^{(k)}_b > 0$ for which the sample yields under the stress state $\boldsymbol{\sigma} = \text{diag}[\sigma^{(k)}_b, t^{(k)}\sigma^{(k)}_b, 0]$, for given stress ratios $t^{(k)}$, that is

$$\sigma^{(k)}_b = \frac{\overline{\sigma}}{f(1, t^{(k)}, 0)} \tag{38}$$

Then, given the set of isotropic generators and the sets of sampling directions θ_p and t_k, the parameters of the yield function, the a_i-coefficients of the linear transformations (33), are identified as the solution of the following optimization problem[16]

$$\text{Min}\ \sqrt{\mathcal{E}_s + \mathcal{E}_r + \mathcal{E}_b} \tag{39}$$

with

$$\mathcal{E}_s := \sum_p\left[w^{t,s}_p\left(\sigma^t_{\theta_p} - \sigma^{t,exp}_{\theta_p}\right)^2 + w^{c,s}_p\left(\sigma^c_{\theta_p} - \sigma^{c,exp}_{\theta_p}\right)^2\right]$$

$$\mathcal{E}_r := \sum_p\left[w^{t,r}_p t\left(r^t_{\theta_p} - r^{t,exp}_{\theta_p}\right)^2 + w^{c,r}_p\left(r^c_{\theta_p} - r^{c,exp}_{\theta_p}\right)^2\right]$$

$$\mathcal{E}_b := \sum_k w_k\left(\sigma^{(k)}_b - \sigma^{(k),exp}_b\right)^2$$

where $\sigma^t_{\theta_p}$, r^t_θ and $\sigma^c_{\theta_p}$, r^c_θ are predicted values according to formulas (36) and (37) in tension and compression,

[13] Assumed to be aligned along the symmetry axes.

[14] One arrives at this parametrization by recalling that the isotropic generators $g^{(i)}$ are pressure-independent.

[15] The angle $\theta \in [0, \pi/2]$ used in this section to indicate directional properties should not be confused with the angle θ on the $\boldsymbol{\pi}$-circle employed in the previous sections.

[16] In fact, a slight variation of this method is used here, see next.

respectively, and $\sigma_b^{(k)}$ are predicted values according to eq.(38); $\sigma_{\theta_p}^{t,exp}$, $\sigma_{\theta_p}^{c,exp}$, etc, are the corresponding values measured from experiments and $w_p^{t,s}$, $w_p^{c,s}$, etc, are weights used in the optimization process.

The number of isotropic generators depends on the level of detail of the experimental characterization. Usually, the directional properties are sampled in three directions, $\theta \in \{0^o, 45^o, 90^o\}$, thus generating 12 data points (yield stresses and r-values in tension and compression). Even if not available, (heuristic) biaxial stress points are in general required to control the shape of biaxial yield curve in the (σ_x, σ_y)-plane. This increases the number of data-points to at least 15. Since each tensor $\boldsymbol{A}$ has five parameters for plane stress states, a number of three isotropic generators (and hence three linear transformations) will be used in eq.(29).

A crucial preliminary step consists in identifying an adequate set of isotropic generators. In general, this may be done by trial and error. Here, given the significant tension/compression asymmetry, this preliminary identification is done by searching for a combination of three generators that provides an optimum transverse isotropic approximation to the data. Thus, with

$$\begin{aligned}
\Sigma_{11} &= b_1\sigma_{11} + b_2\sigma_{22} - (b_1+b_2)\sigma_{33}\\
\Sigma_{22} &= b_2\sigma_{11} + b_1\sigma_{22} - (b_1+b_2)\sigma_{33}\\
\Sigma_{33} &= -\Sigma_{11} - \Sigma_{22}\\
\Sigma_{12} &= (b_1-b_2)\sigma_{12},\ \ \Sigma_{13} = b_3\sigma_{13},\ \ \Sigma_{23} = b_3\sigma_{23}
\end{aligned} \tag{40}$$

representing a generic linear transformation invariant to rotations about the normal (thickness) direction, a subset of the convexity domain, Fig. 4, is investigated:

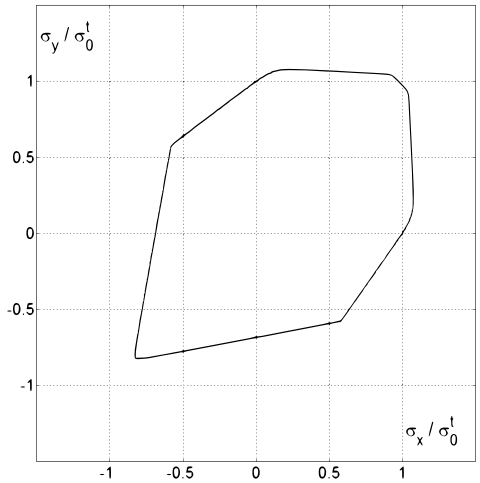

Figure 5: Biaxial curve of the transverse isotropic approximation of the first AZ31 Mg-sheet data set.

given three (t_2, t_3)-points, the optimization problem (39) is solved[17] for $b_k^{(i)}$, $i = 1, 2, 3$, with average directional properties in tension/compression and with the desired shape in the biaxial plane (σ_x, σ_y) as input data and with, for example, $b_1^{(i)} = 2/3, \quad b_2^{(i)} = -1/3, \quad i = 1, 2, 3$ as initial guess (representing isotropy); the most convenient combination of isotropic generators is retained.

Then, the generic orthotropic transformation in eq.(33) is re-parameterized in the form

$$\begin{aligned}
&a_1 = b_1 + c_1,\ \ a_2 = b_2 + c_2\\
&a_3 = b_2 + c_3,\ \ a_4 = b_1 + c_4\\
&a_5 = b_1 - b_2 + c_5,\ \ a_6 = b_3 + c_6,\ \ a_7 = b_3 + c_7
\end{aligned} \tag{41}$$

and the problem (39) is solved for the c_i-parameters (several iterations may be required, but the very first initial guess is, conveniently: $c_k^{(i)} = 0$, $i = 1, 2, 3$).

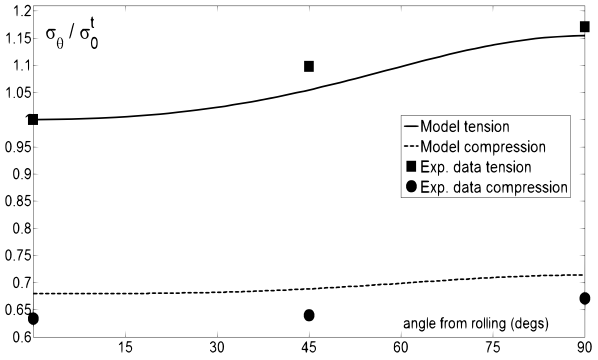

Figure 6: Directional yield stress corresponding to the first AZ31 Mg-sheet data set, data from Lou et al (2007).

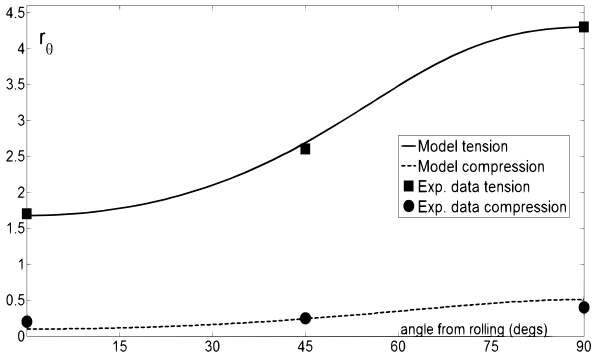

Figure 7: Directional r-values corresponding to the first AZ31 Mg-sheet data set, data from Lou et al (2007).

[17] Solutions to optimization problems reported here have been approximated using the simplex algorithm of Nelder and Mead (1965).

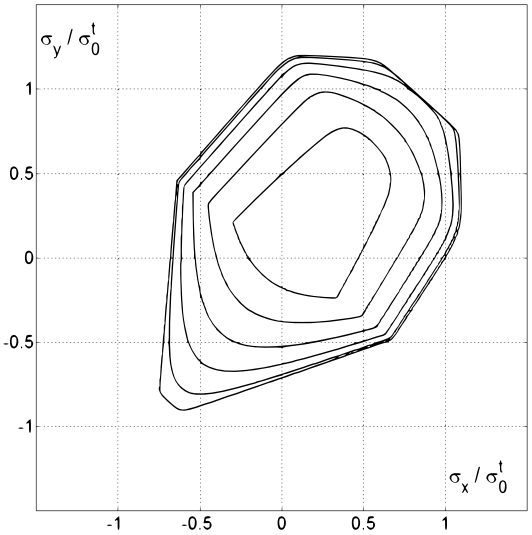

Figure 8: Constant shear sections through the yield surface, of the first model, represented in the biaxial plane (σ_x, σ_y), for $\sigma_{xy}/\sigma_0^t \in \{0, 0.1, 0.2, 0.3, 0.5\}$, the outer curve corresponding to $\sigma_{xy} = 0$.

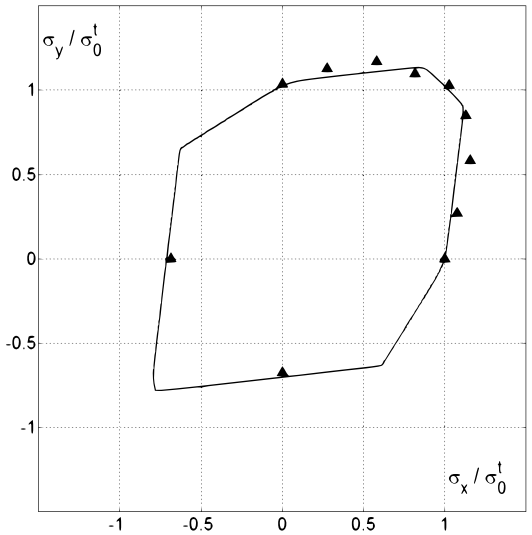

Figure 9: Model 2: biaxial curve and biaxial data reported in Andar et al (2012).

Two experimental characterizations of AZ31B Mg-sheet are considered: one reported in Lou et al (2007), produced by Magnesium Elektron, and the other reported in Andar et al (2012), produced by Posco-Korea. The first data set corresponds to initial yielding, while the second corresponds to a level of 4% of plastic deformation. Notably, for Mg-alloys in general, the *initial* yielding stress in balanced-biaxial tension is less than the tensile yielding stress along the rolling direction; this can be seen in the data reported by Andar et al (2012) and also in the early experimental study of Kelley and Hosford (1968); the situation changes after some deformation, the balanced-biaxial yielding stress becoming greater than the yielding stress along the rolling direction.

The above parameter identification procedure was applied to the modeling of both data sets. Fig. 5 shows the initial transverse isotropic approximation of the data in Lou et al (2007), the average r-value of the model, in tension and compression being 2.139 and 0.225, respectively. The isotropic generators and parameters of the two models are reported in the "Model 1" and "Model 2" columns of Tables C.2-C.4 of Appendix C, for the data in Lou et al (2007) and Andar et al (2012), respectively, and illustrations are shown in Figs. 6-8, and 9-11.

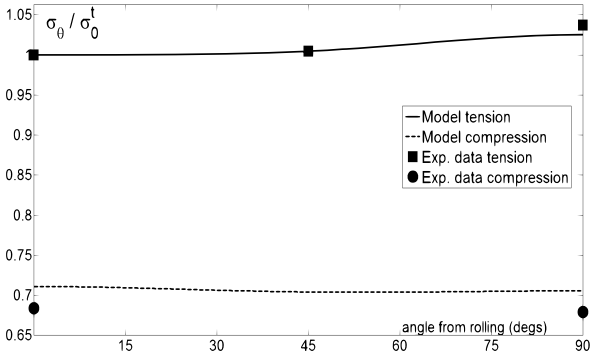

Figure 10: Model 2: directional stresses, data from Andar et al (2012).

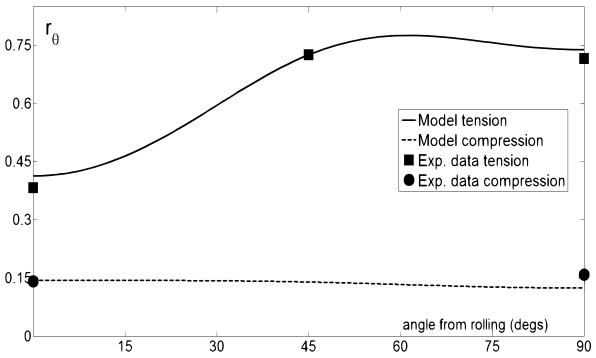

Figure 11: Model 2: directional r-values, data from Andar et al (2012).

Overall, the quality of the two models is satisfactory, the accuracy being good for r-values in both cases, and acceptable for the directional compressive stresses of

the first model. Comparison with other models is hardly possible at this moment, since similar attempts at capturing both biaxial and directional tesnion/compression properties are scarce in the literature[18].

As a final remark, an interesting feature of some of the previously proposed asymmetric functions is that pressure-dependent isotropic functions are used as generators, e.g., Plunkett et al (2008) and Yoon et al (2014). A relative advantage[19] is that the image stresses need not be deviatoric, each having nine parameters for general stress states, instead of the seven parameters of a pressure-independent linear transformation, eq.(33). By using spherical harmonics to represent functions defined on the unit sphere of the space of principal stresses, the present developments extend to pressure-dependent isotropic generators. The corresponding theory and further applications will be reported elsewhere.

Appendix A. Derivatives and convexity of an isotropic function in the natural representation

Formulas for the gradient and Hessian of an isotropic function in the natural representation are presented together with a proof of the convexity condition in eq.(9).

The context being that of eq.(5), the representation

$$f(\boldsymbol{\sigma}) = |\boldsymbol{\sigma}'|h(\theta) = g(\rho,\theta) \tag{A.1}$$

is basically a function of the polar coordinates $\rho = |\boldsymbol{\sigma}'|$ and θ in the deviatoric plane; thus if (x, y) is an associated Cartesian coordinate system, for all points with $x \neq 0$ there holds

$$\rho = (x^2 + y^2)^{1/2}, \quad \tan\theta = y/x \tag{A.2}$$

and

$$x = \rho\cos\theta, \quad y = \rho\sin\theta \tag{A.3}$$

From eq.(8)

$$\cos\theta = \frac{2\sigma_1 - \sigma_2 - \sigma_3}{|\boldsymbol{\sigma}'|\sqrt{6}} \quad \text{and} \quad \sin\theta = \frac{\sigma_2 - \sigma_3}{|\boldsymbol{\sigma}'|\sqrt{2}}$$

so that eq.(A.3) becomes

$$x = \frac{1}{\sqrt{6}}(2\sigma_1 - \sigma_2 - \sigma_3), \quad y = \frac{1}{\sqrt{2}}(\sigma_2 - \sigma_3) \tag{A.4}$$

[18] One may mention the model in Plunkett et al (2008), but comparison is precluded due to the different r-values used as input.

[19] Accurate modeling of the directional properties would still require three linear transformations, since the additional parameters are related to biaxial yielding properties.

Then, from eq.(A.2),

$$\frac{\partial\theta}{\partial x} = \frac{-y}{x^2+y^2}, \quad \frac{\partial\theta}{\partial y} = \frac{x}{x^2+y^2} \tag{A.5}$$

and

$$\frac{\partial\theta}{\partial\sigma_i} = \frac{\partial\theta}{\partial x}\frac{\partial x}{\partial\sigma_i} + \frac{\partial\theta}{\partial y}\frac{\partial y}{\partial\sigma_i} \tag{A.6}$$

together with eq.(A.4) obtain:

$$\begin{aligned}
\frac{\partial\theta}{\partial\sigma_1} &= \frac{\sigma_3 - \sigma_2}{|\boldsymbol{\sigma}'|^2\sqrt{3}} \\
\frac{\partial\theta}{\partial\sigma_2} &= \frac{\sigma_1 - \sigma_3}{|\boldsymbol{\sigma}'|^2\sqrt{3}} \\
\frac{\partial\theta}{\partial\sigma_3} &= \frac{\sigma_2 - \sigma_1}{|\boldsymbol{\sigma}'|^2\sqrt{3}}
\end{aligned} \tag{A.7}$$

Then the gradient of the function in eq.(A.1),

$$\frac{\partial f}{\partial\sigma_i} = \frac{\partial\rho}{\partial\sigma_i}h(\theta) + \rho\, h'(\theta)\frac{\partial\theta}{\partial\sigma_i} \tag{A.8}$$

is calculated with the help of

$$\frac{\partial\rho}{\partial\sigma_i} = \frac{\partial|\boldsymbol{\sigma}'|}{\partial\sigma_i} = \frac{\sigma_i'}{|\boldsymbol{\sigma}'|} \tag{A.9}$$

and of eq.(A.7), as

$$\begin{aligned}
\frac{\partial f}{\partial\sigma_1} &= \frac{1}{|\boldsymbol{\sigma}'|}\left[\sigma_1'\, h(\theta) + \frac{\sigma_3 - \sigma_2}{\sqrt{3}}h'(\theta)\right] \\
\frac{\partial f}{\partial\sigma_2} &= \frac{1}{|\boldsymbol{\sigma}'|}\left[\sigma_2'\, h(\theta) + \frac{\sigma_1 - \sigma_3}{\sqrt{3}}h'(\theta)\right] \\
\frac{\partial f}{\partial\sigma_3} &= \frac{1}{|\boldsymbol{\sigma}'|}\left[\sigma_3'\, h(\theta) + \frac{\sigma_2 - \sigma_1}{\sqrt{3}}h'(\theta)\right]
\end{aligned} \tag{A.10}$$

Taking partial derivatives in eq.(A.8) obtains

$$\begin{aligned}
\frac{\partial^2 f}{\partial\sigma_i\partial\sigma_j} &= \frac{\partial^2|\boldsymbol{\sigma}'|}{\partial\sigma_i\partial\sigma_j}h(\theta) + |\boldsymbol{\sigma}'|h''(\theta)\frac{\partial\theta}{\partial\sigma_i}\frac{\partial\theta}{\partial\sigma_j} \\
&+h'(\theta)\left[\frac{\partial|\boldsymbol{\sigma}'|}{\partial\sigma_i}\frac{\partial\theta}{\partial\sigma_j} + \frac{\partial|\boldsymbol{\sigma}'|}{\partial\sigma_j}\frac{\partial\theta}{\partial\sigma_i} + |\boldsymbol{\sigma}'|\frac{\partial^2\theta}{\partial\sigma_i\partial\sigma_j}\right]
\end{aligned} \tag{A.11}$$

From eq.(A.9) one calculates

$$\frac{\partial^2|\boldsymbol{\sigma}'|}{\partial\sigma_i\partial\sigma_j} = \frac{1}{|\boldsymbol{\sigma}'|}\left(\delta_{ij} - \frac{1}{3} - \frac{\sigma_i'\sigma_j'}{|\boldsymbol{\sigma}'|^2}\right) \tag{A.12}$$

For example, for $i = 1$ and $j = 1$, after using the relationship $\sigma_1' + \sigma_2' + \sigma_3' = 0$:

$$\frac{\partial^2|\boldsymbol{\sigma}'|}{\partial\sigma_1\partial\sigma_1} = \frac{(\sigma_3 - \sigma_2)^2}{3|\boldsymbol{\sigma}'|^3}$$

and then, with eq.(A.7) one obtains:

$$|\boldsymbol{\sigma}'|\frac{\partial\theta}{\partial\sigma_1}\frac{\partial\theta}{\partial\sigma_1} = \frac{(\sigma_3 - \sigma_2)^2}{3|\boldsymbol{\sigma}'|^3} = \frac{\partial^2|\boldsymbol{\sigma}'|}{\partial\sigma_1\partial\sigma_1}$$

Similar calculations show that the above relationship holds for all pair of indices, that is:

$$|\boldsymbol{\sigma}'|\frac{\partial\theta}{\partial\sigma_i}\frac{\partial\theta}{\partial\sigma_j} = \frac{\partial^2|\boldsymbol{\sigma}'|}{\partial\sigma_i\partial\sigma_j} \tag{A.13}$$

Next, from eq.(A.7):

$$\frac{\partial^2\theta}{\partial\sigma_1\partial\sigma_1} = \frac{2\sigma_1'(\sigma_2-\sigma_3)}{|\boldsymbol{\sigma}'|^4\sqrt{3}}$$

and hence, with eqs.(A.9) and (A.7):

$$\frac{\partial|\boldsymbol{\sigma}'|}{\partial\sigma_1}\frac{\partial\theta}{\partial\sigma_1} + \frac{\partial|\boldsymbol{\sigma}'|}{\partial\sigma_1}\frac{\partial\theta}{\partial\sigma_1} + |\boldsymbol{\sigma}'|\frac{\partial^2\theta}{\partial\sigma_1\partial\sigma_1} = 0$$

Similar calculations show that the above relation holds for all pairs of indices, that is:

$$\frac{\partial|\boldsymbol{\sigma}'|}{\partial\sigma_i}\frac{\partial\theta}{\partial\sigma_j} + \frac{\partial|\boldsymbol{\sigma}'|}{\partial\sigma_j}\frac{\partial\theta}{\partial\sigma_i} + |\boldsymbol{\sigma}'|\frac{\partial^2\theta}{\partial\sigma_i\partial\sigma_j} = 0 \tag{A.14}$$

From eqs.(A.11), (A.13) and (A.14) one obtains

$$\frac{\partial^2 f}{\partial\sigma_i\partial\sigma_j} = \left[h''(\theta)+h(\theta)\right]\frac{\partial^2|\boldsymbol{\sigma}'|}{\partial\sigma_i\partial\sigma_j} \tag{A.15}$$

Formulas (A.10) and (A.15) feature the gradient and the Hessian of an isotropic pressure-independent homogeneous function in the natural representation (A.1). Formula (A.15) is particularly interesting: it shows that calculating the Hessian of an arbitrary isotropic function is not much more complicated than calculating the Hessian of the von Mises function. In addition, since the latter is convex, it follows that the function f is convex[20] if and only if

$$h''(\theta)+h(\theta)\geq 0,\quad \forall\theta\in[0,\pi/3]$$

which is the convexity condition stated in eq.(9).

Appendix B. The gradient of an anisotropic extension

It is sufficient to consider the case of a single isotropic generator, thus functions of the form

$$f(\boldsymbol{\sigma}) = g(\Sigma_1,\Sigma_2,\Sigma_3)$$

where Σ_p are the principal stresses of the image stress $\boldsymbol{\Sigma} = \boldsymbol{A}:\boldsymbol{\sigma}$. With σ_{ij} denoting components of the stress $\boldsymbol{\sigma}$ with respect to an arbitrary orthonormal basis, the above representation implies

$$\frac{\partial f}{\partial\sigma_{ij}} = \sum_p \frac{\partial g}{\partial\Sigma_p}\frac{\partial\Sigma_p}{\partial\sigma_{ij}} \tag{B.1}$$

The gradient $\partial g/\partial\Sigma_p$ is calculated using eq.(A.10) of Appendix A. It remains to deduce formulas for the calculation of[21] $\partial\Sigma_p/\partial\sigma_{ij}$.

Eq.(34) is well-suited for calculating the principal values of a symmetric tensor in terms of its components with respect to an orthogonal basis. On the other hand, ±1 are singular points for the derivative of the acos-function and hence "branches" seem inherent when calculating gradients. Then a slightly more efficient approach is to start directly from the equation characterizing the principal values of the *deviatoric* stress $\boldsymbol{\Sigma}$:

$$\Sigma_p^3 - J_2\Sigma_p - J_3 = 0$$

Differentiation with respect with respect to σ_{ij} obtains

$$\left(3\Sigma_p^2 - J_2\right)\frac{\partial\Sigma_p}{\partial\sigma_{ij}} = \frac{\partial J_2}{\partial\sigma_{ij}}\Sigma_p + \frac{\partial J_3}{\partial\sigma_{ij}}$$

Recalling the definition of J_2 in eq.(35) and that $\Sigma_1+\Sigma_2+\sigma_3=0$, there holds

$$3\Sigma_p^2 - J_2 = \begin{cases} 2\Sigma_1^2-\Sigma_2^2-\Sigma_1\Sigma_2, & \text{if } p=1\\ -\Sigma_1^2+2\Sigma_2^2-\Sigma_1\Sigma_2, & \text{if } p=2\\ 2\Sigma_1^2+2\Sigma_2^2+5\Sigma_1\Sigma_2, & \text{if } p=3\end{cases}$$

and hence

$$3\Sigma_1^2 - J_2 = 0 \iff \Sigma_1=\Sigma_2 \text{ or } \Sigma_2=-2\Sigma_1$$

$$3\Sigma_2^2 - J_2 = 0 \iff \Sigma_1=\Sigma_2 \text{ or } \Sigma_1=-2\Sigma_2$$

$$3\Sigma_1^3 - J_2 = 0 \iff \Sigma_1=-2\Sigma_2 \text{ or } \Sigma_2=-2\Sigma_1$$

Then the sought gradients are calculated as follow:
(1) If $\Sigma_1\neq\Sigma_2$ and $\Sigma_2\neq-2\Sigma_1$ and $\Sigma_1\neq-2\Sigma_2$, then $3\Sigma_p^2-J_2\neq0$, for $p=1,2,3$, and then

$$\frac{\partial\Sigma_p}{\partial\sigma_{ij}} = \frac{1}{3\Sigma_1^2-J_2}\left(\frac{\partial J_2}{\partial\sigma_{ij}}\Sigma_p + \frac{\partial J_3}{\partial\sigma_{ij}}\right),\quad p=1,2,3$$

[20] An alternative argument makes use of a theorem of Davis (1957): a numerical function $f=f(M)$ defined over a space of symmetric matrices and depending only on the spectrum of the matrix in the form $f(M)=g(m_1,...,m_n)$, where m_i are the eigenvalues of M, is convex if and only if the function g is symmetric and convex. Then, a direct verification shows that the matrix $\partial^2|\boldsymbol{\sigma}'|/\partial\sigma_i\partial\sigma_j$ is positive definite and hence the function $f=f(\sigma_1,\sigma_2,\sigma_3)$ is convex over subsets of the 3D-space of vectors $(\sigma_1,\sigma_2,\sigma_3)$; by Davis'theorem, f will be convex also as a function over the space of stress tensors.

[21] In particular, if $\boldsymbol{A}$ is the restriction of the fourth order identity tensor to the subspace of deviatoric tensors, $\partial\Sigma_p/\partial\sigma_{ij}$ reduces to $\partial\sigma_p'/\partial\sigma_{ij}$ and eq.(B.1) becomes a general formula for the gradient of an isotropic function with respect to the components of its argument.

(2) If $\Sigma_1 = \Sigma_2$, then $3\Sigma_3^2 - J_2 \neq 0$, and then

$$\frac{\partial \Sigma_3}{\partial \sigma_{ij}} = \frac{1}{3\Sigma_3^2 - J_2}\left(\frac{\partial J_2}{\partial \sigma_{ij}}\Sigma_3 + \frac{\partial J_3}{\partial \sigma_{ij}}\right)$$

and, since $\Sigma_3 = -\Sigma_1 - \Sigma_2 = -2\Sigma_1 = -2\Sigma_2$,

$$\frac{\partial \Sigma_p}{\partial \sigma_{ij}} = -\frac{1}{2}\frac{\partial \Sigma_3}{\partial \sigma_{ij}}, \quad p = 1, 2$$

(3) If $\Sigma_2 = -2\Sigma_1$, then $3\Sigma_2^2 - J_2 \neq 0$, and then

$$\frac{\partial \Sigma_2}{\partial \sigma_{ij}} = \frac{1}{3\Sigma_2^2 - J_2}\left(\frac{\partial J_2}{\partial \sigma_{ij}}\Sigma_2 + \frac{\partial J_3}{\partial \sigma_{ij}}\right)$$

$$\frac{\partial \Sigma_p}{\partial \sigma_{ij}} = -\frac{1}{2}\frac{\partial \Sigma_2}{\partial \sigma_{ij}}, \quad p = 1, 3$$

(4) If $\Sigma_1 = -2\Sigma_2$, then $3\Sigma_1^2 - J_2 \neq 0$, and then

$$\frac{\partial \Sigma_1}{\partial \sigma_{ij}} = \frac{1}{3\Sigma_1^2 - J_2}\left(\frac{\partial J_2}{\partial \sigma_{ij}}\Sigma_1 + \frac{\partial J_3}{\partial \sigma_{ij}}\right)$$

$$\frac{\partial \Sigma_p}{\partial \sigma_{ij}} = -\frac{1}{2}\frac{\partial \Sigma_1}{\partial \sigma_{ij}}, \quad p = 2, 3$$

Finally, for completeness, the gradients of J_2 and J_3 are, generically:

$$\frac{\partial J}{\partial \sigma_{ij}} = \sum_{a,b} \frac{\partial J}{\partial \Sigma_{ab}}\frac{\partial \Sigma_{ab}}{\partial \sigma_{ij}}$$

where, with the usual vectorization of stress tensors,

$$\frac{\partial J_2}{\partial \Sigma_{ab}} = (\Sigma_{11}, \Sigma_{22}, \Sigma_{33}, 2\Sigma_{12}, 2\Sigma_{13}, 2\Sigma_{13})^T$$

$$\frac{\partial J_3}{\partial \Sigma_{ab}} = [\Sigma_{22}\Sigma_{33} - \Sigma_{23},\ \Sigma_{11}\Sigma_{33} - \Sigma_{13},\ \Sigma_{11}\Sigma_{22} - \Sigma_{12},$$
$$2(\Sigma_{13}\Sigma_{23} - \Sigma_{12}\Sigma_{33}),\ 2(\Sigma_{12}\Sigma_{23} - \Sigma_{13}\Sigma_{22}),$$
$$2(\Sigma_{12}\Sigma_{13} - \Sigma_{23}\Sigma_{11})]^T$$

and, from eq.(33),

$$\frac{\partial \Sigma_{11}}{\partial \sigma_{ij}} = (a_1,\ a_2,\ -a_1 - a_2,\ 0,\ 0,\ 0)^T$$

$$\frac{\partial \Sigma_{22}}{\partial \sigma_{ij}} = (a_3,\ a_4,\ -a_3 - a_4,\ 0,\ 0,\ 0)^T$$

$$\frac{\partial \Sigma_{33}}{\partial \sigma_{ij}} = -\left(\frac{\partial \Sigma_{11}}{\partial \sigma_{ij}} + \frac{\partial \Sigma_{22}}{\partial \sigma_{ij}}\right)$$

$$\frac{\partial \Sigma_{12}}{\partial \sigma_{ij}} = (0,\ 0,\ 0,\ a_5,\ 0,\ 0)^T$$

$$\frac{\partial \Sigma_{13}}{\partial \sigma_{ij}} = (0,\ 0,\ 0, 0,\ a_6,\ 0)^T$$

$$\frac{\partial \Sigma_{23}}{\partial \sigma_{ij}} = (0,\ 0,\ 0,\ 0,\ 0,\ a_7)^T$$

Appendix C. Tables of numerical parameters

Table C.1: Numerical values of the a_i parameters of the trigonometric representation in eq.(6).

	CPB	HH	Poly6
a_0	3.43878513	2.64295225	3.71812212
a_1	-0.39425458	0.0	-0.44949023
a_2	-0.06978321	-0.07183851	-0.09665677
a_3	-0.02020266	0.0	-0.03909226
a_4	-0.00660238	-0.01521937	-0.01985927
a_5	-0.00231523	0.0	-0.01128121
a_6	-0.00088558	-0.00537965	-0.00680347
a_7	-0.00035950	0.0	-0.00423302
a_8	-0.00014405	-0.00226389	-0.00266788
a_9	-0.00005673	0.0	-0.00168074
a_{10}	-0.00002442	-0.00103420	-0.00104690
a_{11}	-0.00001143	0.0	-0.00063820
a_{12}	-0.00000468	-0.00049510	-0.00037676
a_{13}	-0.00000159	0.0	-0.00021283
a_{14}	-0.00000081	-0.00024436	-0.00011347
a_{15}	-0.00000057	0.0	-0.00005632
a_{16}	-0.00000019	-0.00012326	-0.00002603
a_{17}		0.0	-0.00001207
a_{18}		-0.00006320	-0.00000732

Table C.2: Numerical values of the t_2 and t_3 shape-parameters characterizing the isotropic generators by eqs.(14) and (16).

	Model 1	Model 2
$t_2^{(1)}$	1.82378	1.83030
$t_3^{(1)}$	1.37086	1.37410
$t_2^{(2)}$	1.82378	1.78469
$t_3^{(2)}$	1.37077	1.35145
$t_2^{(3)}$	1.83030	1.81727
$t_3^{(3)}$	1.37410	1.36686

Table C.3: Numerical values of the b_i parameters of the transverse isotropic linear transformations in eq.(40).

	Model 1	Model 2
$b_1^{(1)}$	0.62244648	-0.94934324
$b_2^{(1)}$	-0.35794805	-0.94921488
$b_1^{(2)}$	0.49789902	1.68358706
$b_2^{(2)}$	-0.47899704	-1.63654452
$b_1^{(3)}$	-0.26570862	1.28981641
$b_2^{(3)}$	-0.26720922	-0.71132313

Table C.4: Numerical values of the c_i parameters of the orthotropic linear transformations in eq.(41).

	Model 1	Model 2
$c_1^{(1)}$	0.15753363	0.08974462
$c_2^{(1)}$	0.07057620	0.13001845
$c_3^{(1)}$	-0.08794903	0.09471368
$c_4^{(1)}$	-0.08147106	0.12176141
$c_5^{(1)}$	0.02637219	0.10552885
$c_1^{(2)}$	-0.01107806	0.14658043
$c_2^{(2)}$	0.10060782	-0.03189079
$c_3^{(2)}$	0.02425665	-0.11177784
$c_4^{(2)}$	0.00170572	0.18749099
$c_5^{(2)}$	-0.03097213	0.24100154
$c_1^{(3)}$	0.07828269	-0.24215285
$c_2^{(3)}$	0.00640890	0.13660833
$c_3^{(3)}$	0.07995998	0.21262800
$c_4^{(3)}$	0.00490868	-0.17721402
$c_5^{(3)}$	-0.00146543	-0.33462270

Acknowledgement. This work was supported by Qatar National Research Fund through the NPRP grants # 09-611-2-236 and # 4-1411-2-555. The statements made herein are solely the responsibility of the authors.

References

Andar, M.O., Kuwabara, T., Steglich, D., 2012. Material modeling of AZ31 Mg sheet considering variation of r-values and asymmetry of the yield locus. Mat. Sci. Eng. A, 549, 82-92.

Balasubramanian, S., Anand, L., 2002. Plasticity of initially textured hexagonal polycrystals at high homologous temperatures: application to titanium. Acta Mat., 50, 133-148.

Banabic, D., Aretz, H., Comsa, S., Paraianu, L., 2005. An improved analytical description of orthotropy in metallic sheets. Int. J. Plast., 21, 493-512.

Barlat, F., Aretz, H., Yoon, J.W., Karabin, M.E., Brem, J.C., Dick, R.E., 2005. Linear transformation based anisotropic yield function. Int. J. Plast., 21, 1009-1039.

Barlat, F., Yoon, J.W., Cazacu, O., 2007. On linear transformations of stress tensors for the description of plastic anisotropy. Int. J. Plast., 23, 876-896.

Barlat, F., Gracio, J.J., Lee, M.G., Rauch, E.F., Vincze, G., 2011. An alternative to kinematic hardening in classical plasticity. Int. J. Plast., 27, 1309-1327.

Bilby, B.A., Crocker, A.G., 1965. The theory of the crystallography of deformation twinning. Proc. R. Soc. Lond. A, 288, no. 1413, 240-255.

Budianski, B., 1984. Anisotropic plasticity of plane-isotropic sheets. In Mechanics of Material Behavior, Dvorak G.J. and Shield R.T., eds, pp 15-29. Elsevier, Amsterdam.

Cazacu, O., Barlat, F., 2004. A criterion for description of anisotropy and yield differential effects in pressure-insensitive metals. Int. J. Plast., 20, 2027-2045.

Cazacu, O., Plunkett, B., Barlat, F., 2006. Othotropic yield criterion for hexagonal closed packed metals. Int. J. Plast., 22, 1171-1194.

Christian, J.W., Mahajan, S., 1995. Deformation twinning. Prog. Mat. Sci., 39, 1-157.

Davis, C., 1957. All convex invariant functions of hermitian matrices. Arch. Math., 8, 276-278.

Graff, S., Brocks, W., Steglich, D., 2007. Yielding of magnesium: From single crystal to polycrystalline aggregates. Int. J. Plast., 23, 1957-1978.

Hershey, A.V., 1954. The plasticity of an isotropic aggregate of anisotropic face centered cubic crystals. J. Appl. Mech., 21, 241-249.

Hill, R., 1950. The mathematical theory of plasticity. Clarendon Press, Oxford. Ch. 1.

Hosford, W.F., 1972. A generalized isotropic yield criterion. J. Appl. Mech., 39, 607-609.

Huang, M, Man, C.-S., 2013. A generalized Hosford yield function for weakly-textured sheets of cubic metals. Int. J. Plast., 41, 97-123.

Karafillis, A.P., Boyce, M.C., 1993. A general anisotropic yield criterion using bounds and a transformation weighting tensor. J. Mech. Phys. Solids, 41, 1859-1886.

Kelley, E.W., Hosford, W.F., 1968. Deformation characteristics of textured magnesium. Trans. TMSAIME 242, 654661.

Kouchmeshky, B., Zabaras, N., 2009. Modeling the response of HCP polycrystals deforming by slip and twinning using a finite element representation of the orientation space. Comp. Mat. Sci., 45, 1043-1051.

Liu, C., Huang, Y., Stout, M.G., 1997. On the asymmetric yield surface of plastically orthotropic materials: a phenomenological study. Acta Mater., 45, 2397-2406.

Lou, X.Y., Li, M., Boger, R.K., Agnew, S.R., Wagoner, R.H., 2007. Hardening evolution of AZ31B Mg sheet. Int. J. Plast., 23, 44-86.

Malvern, L.E., 1969. Introduction to the mechanics of a continuous medium. Prentice-Hall, Englewood Cliffs, N.Y. Ch. 3.

Nelder, J.A., Mead, R., 1965. A simplex method for function minimization. The Comp. J., 7, 308-313.

Ortiz, M., Popov, E.P., 1983. Distortional hardening rules for metal plasticity. J. Eng. Mech., 109, 1042-1057.

Plunkett, B., Cazacu, O., Barlat, F., 2008. Orthotropic yield criteria for description of the anisotropy in tension and compression of sheet metals. Int. J. Plast., 24, 847-866.

Soare, S.C., Yoon, J.W., Cazacu, O., 2007. On using homogeneous polynomials to design anisotropic yield functions with tension/compression symmetry/asymmetry. In: Cesar de Sa, JMA, Santos AD (eds) Materials processing and design: modeling, simulation and Applications. Proc. of the NUMIFORM 2007 Conf., Porto, 607-612.

Soare, S.C., Barlat, F., 2010. Convex polynomial yield functions. J. Mech. Phys. Solids, 58, 1804-1818.

Yoon, J.W., Lou, Y., Yoon, J., Glazoff, M.V., 2014. Asymmetric yield function based on the stress invariants for pressure sensitive metals. Int. J. Plast., 56, 184-202.

Zatarin, P., Lipinski, P., Rosochowski, A., 2004. Numerical study of the influence of microstructure on subsequent yield surfaces of polycristalline materials. Int. J. Mech. Sci., 46, 1377-1398.